Journal of Materials Chemistry A

ARTICLE

Supporting Information

Ultra-highly conductive hollow channels guided by a bamboo bio-template for electric and electrochemical devices

Prof. Dr. Omar G. Pandoli[1]*, Reginaldo J.G. Neto[2], Natália R. Oliveira[2], Ana C. Fingolo[2], Dra Cátia C. Corrêa[2], Prof, Dr. Khosrow Ghavami[3], Prof. Dr. Mathias Strauss[2,4]*, Prof. Dr. Murilo Santhiago[2,4]*

1 - Department of Chemistry, Pontifícia Universidade Católica do Rio de Janeiro, Rua Marques de São Vicente, Zipe Code 22451-900, Rio de Janeiro, Brazil.
E-mail: omarpandoli@puc-rio.br
2 - Brazilian Nanotechnology National Laboratory (LNNano), Brazilian Center for Research in Energy and Materials (CNPEM), Zip Code 13083-970, Campinas, São Paulo, Brazil.
3- Department of Civil Engineering, Pontifícia Universidade Católica do Rio de Janeiro, Rua Marques de São Vicente, Zipe Code 22451-900, Rio de Janeiro, Brazil.
4 - Center of Natural and Human Sciences, Federal University of ABC, Zip Code 09210-580, Santo André, São Paulo Brazil.
E-mail: mathias.strauss@lnnano.cnpem.br; murilo.santhiago@lnnano.cnpem.br

A) Distance/gap between electrodes

Figure S1 shows an optical microscope image of the bottom face of the fully-integrated device before the addtion of the Al wires. The distance between electrodes were kept aproximatelly in the range of 500 – 1000 µm to avoid short circuit and at the sime time maximize the number of electrodes in the BEC.

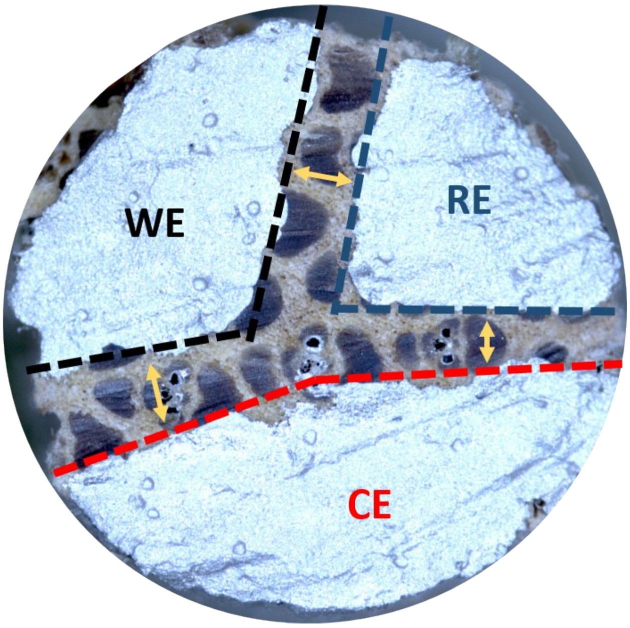

Figure S1. Stereomicroscope images of the bottom face of bamboo in the fully-integrated configuration. The yellow arrows shows the typical distance of the electrodes, in the range of 700 (±249) µm.

B) Schematic fabrication process of the fully-integrated three-electrodes into bamboo

Figure S2 desribes the main steps involving the fabrication of the 3D bamboo fully-integrated electrochemical cell (BEC).

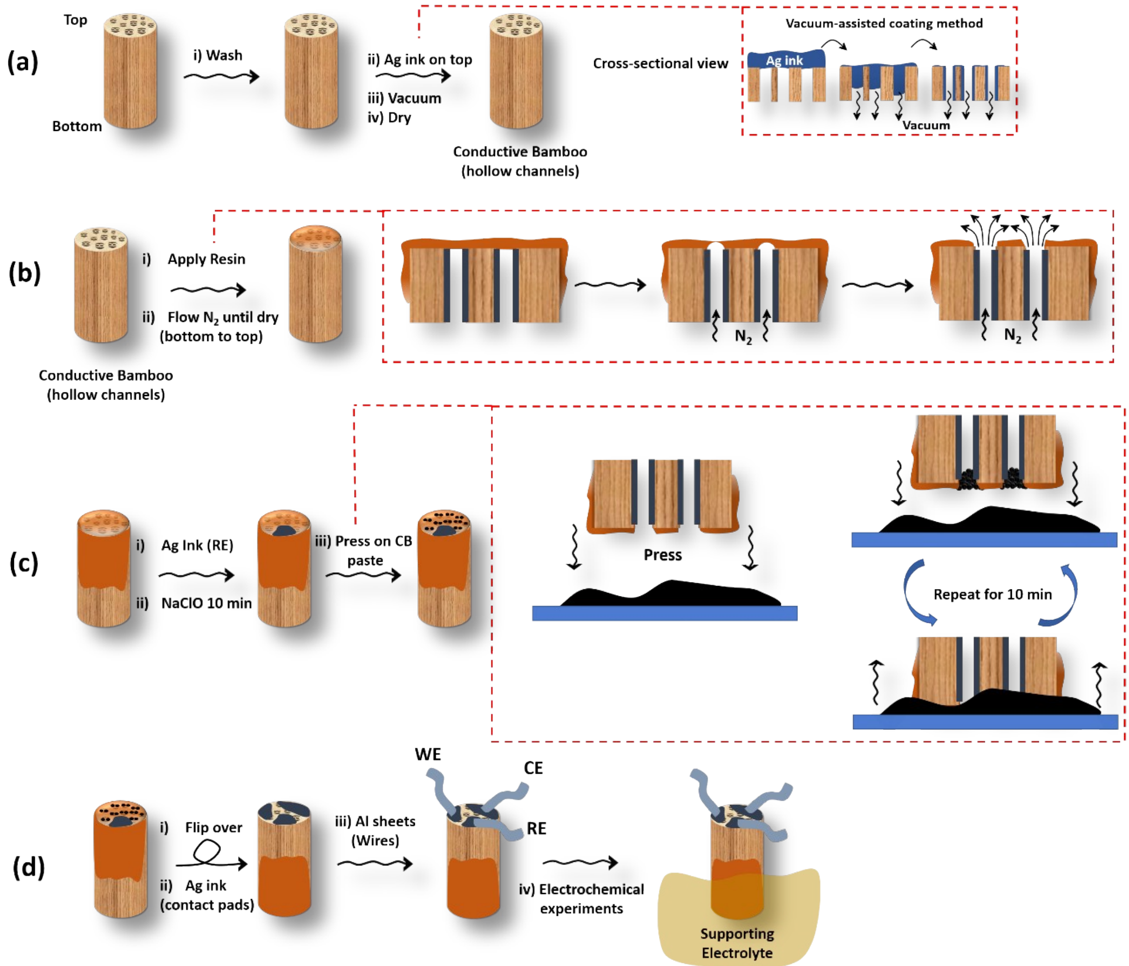

Figure S2. a) After cut, bamboo specimen is washed and filled with silver ink to obtain hollow conductive microchannels. b) Epoxy resin is added on the top surface and N_2 is flowed through the channels from bottom to top. c) Ag ink is patterned and treated with NaClO to obtain the reference electrode. The top surface is the consecutively pressed on the carbon black paste previously added on a flat surface, as schematically shown. d) Electrical contact pads are patterned on the bottom surface and the bamboo is imersed in the supporting electrolyte for the electrochemical experiments.

C) Porosity and density values of bamboo

Porosity and density values of bamboo and Ag-coated bamboo are presented on Table S1 below. Materials porosity was calculated from μCT data. Natural washed bamboo sample presented a porosity of 25.9 (±0.2)% and modified bamboo 25.7 (±0.9)%, as shown in Table S1. Negligible reduction on modified bamboo porosity compared to natural bamboo may be related to two factors: i) silver coating is too thin that changes fall below μCT detection limit, and ii) calculated porosity considers not only bamboo channels but also the overall porosity from parenchyma and sclerenchyma tissues.

Apparent density values of materials are also presented in Table S1 below. A slight increase on density is observed for the Ag-coated sample but statistically irrelevant, indicating that our process practically preserves the density of the natural bamboo specimen.

Table S1. Porosity and density values of bamboo and Ag-coated bamboo.

Material	Porosity (%)[a]	Density (g cm^{-3})[b]
Bamboo	25.9 ($\pm$ 0.2)	0.78 ($\pm$ 0.03)
Ag-coated bamboo	25.7 ($\pm$ 0.9)	0.81 ($\pm$ 0.06)

[a]Calculated from μCT data. Average of 5 regions.
[b]Apparent density calculated from samples mass and volume values (cylindric pieces). Average of 5 pieces

D) Thickness of the conductive coating

We calculated the thickness of the Ag coating using laser scanning confocal microscopy (Figure S3). The mean value was calculated using different regions of the sample.

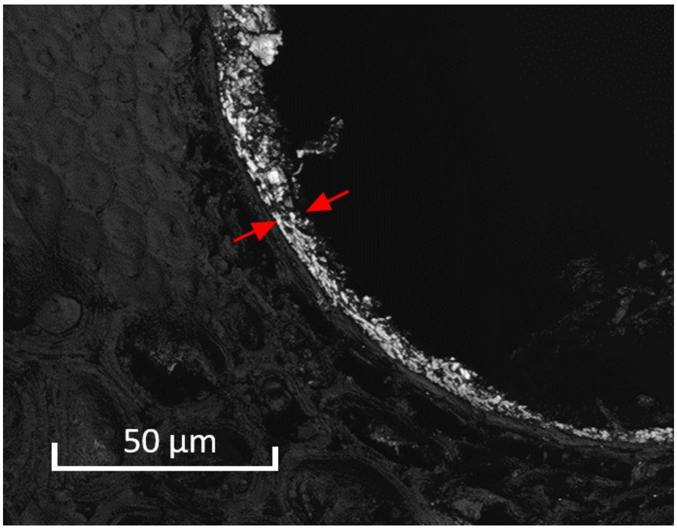

Figure S3. Laser scanning confocal image of the Ag-coated bamboo. The thickness in the selected region is 10.5 µm.

We also measured the conductivity of a silver track patterned directly on a hydrophilic glass substrate using the same ink. We used sacrificial adhesive layers to create conductive tracks of 0,2 x 3 cm (w × L) as reported by us recently.[1,2] The conductivity of silver tracks on glass was 9.2 (±2.0)$\times 10^5$ S m^{-1}, which is in good agreemnt with Ag-coated bamboo microchannels. The thickness of the tracks was aproximatelly 15 µm.

As can be shown in table S2 below, the materials presented in entrys (g) and (j) have superior conductivity when compared with the proposed route (entry (e)). However, the patterning routes are not compatible with the structure of bamboo. For instance, the route described in entry (g) requires a flash reduction of the metal ions. Since bamboo is not transparent to UV-visible light, the reduction will not occur inside of the microchannels. Entry (j) also describe a carbon-based material with high conductivity, however, the authors reported the fabrication of carbon fibers for functional applications. The fibers have a diameter of ~25 µm, which are lower than the diameter of the bamboo channels. However, fill several centimeter long bamboo-channels with these fibers is far away to be scalable and a fast patterning route. Moreover, it will require a micromanipulator to introduce the fibers inside of the bamboo-based channels.

Table S2. Comparison Table.

Entry	Methodology /Materials	Conductivity [S m^{-1}]
(a)[3]*	Microcoils were aligned in a PDMS matrix using AC electric field.	10
(b)[4]*	Cured graphite nanoplateled dispersion pressed between glass slides.	4.5×10^2
(c)[5]*	Incorporation of Sn-Bi alloy in wood channels.	5.4×10^4
(d)[6]*	Aligned carbon nanotubes usign a filtration process.	2.5×10^5
(e)This* work	Vaccum-assited Ag coating method in highly oriented bamboo channels.	9.4×10^5
(f)[7]	Evaporation-induced sintering of liquid metal droplets (LMD).	2.0×10^5
(g)[8]	Metal ink using particle-free reactive silver ink.	2.4×10^7
(h)[9]	Graphene paper prepared by ball-milling, filtration, annealing, and compression	2.2×10^5
(i)[10]	Screen-printed multi-layer graphene ink using cellulose-derived solvent	7.1×10^4
(j)[11]	Iodine-doped carbon nanotube fibers	5.0×10^6

* Conductivity in aligned materials ($\sigma_{||}$) .

E) Additional characterization of bamboo and Ag-coated bamboo

Scanning electron images of bamboo and Ag-coated bamboo under 150, 500 and 1000x magnification are present below.

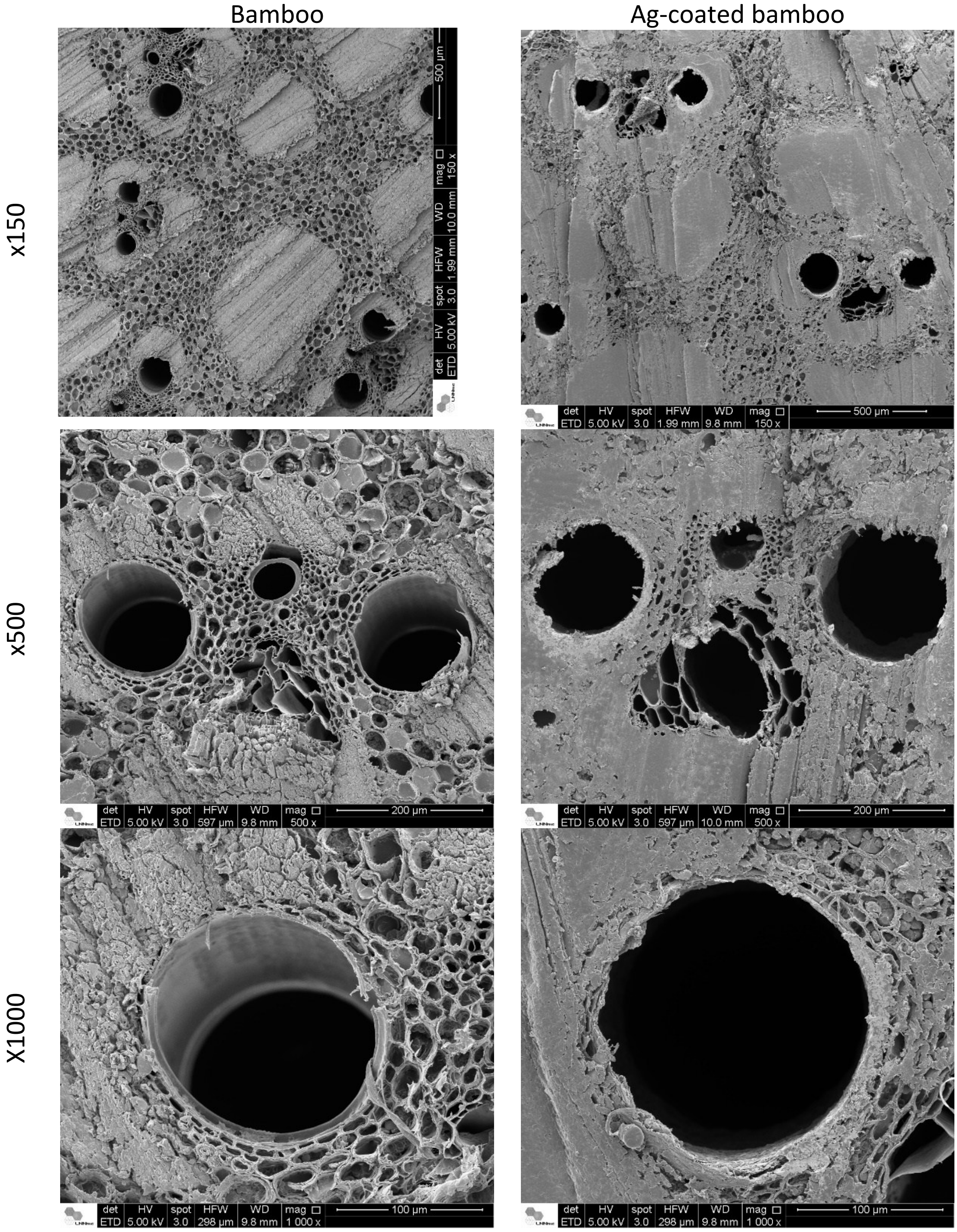

Figure S4. Scanning electron images of bamboo and Ag-coated bamboo.

F) Photos of the 3D circuit

Figure S5 shows the photos of the electrical contacts pads of each bamboo especimen.

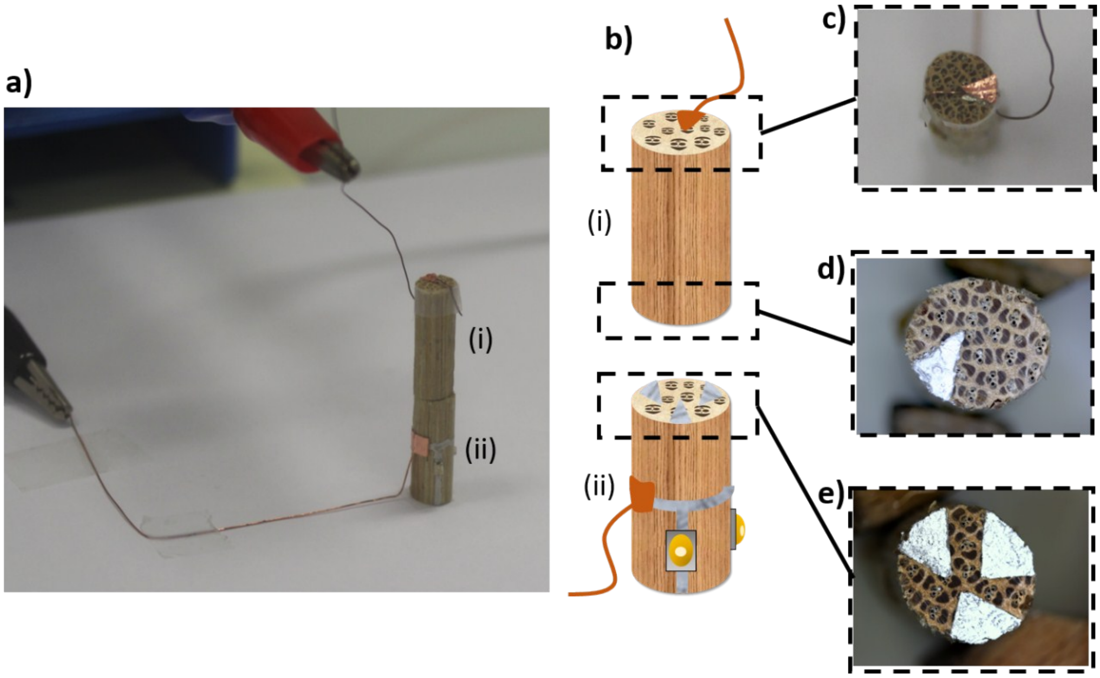

Figure S5. a) Photo of the assembled device. (b) Schematic view of the two pieces of bamboo used to fabricate the 3D electrical device. c-e) Photo of the electrical contact pads. The bottom face of bamboo (ii) follows the same electrical pattern illustrated in Figure S1(e).

G) Determination of the energy efficiency

The heat transferred to the water, Q_w, in the bamboo section was calculated as follows:

$$Q_w(W) = m * C_{p,\,ave} * (T_{out} - T_{in}) \,, \qquad \text{(Eq. S1)}$$

where m is the water flow rate, $C_{p,ave}$ is the average specific heat of the water, and T_{out} and T_{in} are the average outlet and inlet temperatures of the water, respectively.
The $C_{p,ave}$ was calculated according to the following Equation (5),

$$C_{p,\,ave}\left(\frac{J}{kmol}.K\right) = \frac{\int_{T_{in}}^{T_{out}} C_p(T) \times dT}{T_{out} - T_{in}} \,, \qquad \text{(Eq. S2)}$$

Where,

$$Cp(T)\left(\frac{J}{kmol}.K\right) = 3.17 \times 10^6 - 7.26 \times 10^6 \times T + 8.54 \times 10^6 \times T^2 - 4.49 + 9.01 \times 10^5 \times T^4 \qquad \text{(Eq. S3)}$$

12

The power supplied by the source, P, was calculated from the source voltage, V, and current, I, as follows,

$$P\,(W) = V * I \,, \qquad \text{(Eq. S4)}$$

Then, the energy efficiency, EE, of the system was calculated as the ratio between the heat transfer to the water and the power supplied by the source, as follows,

$$EE\,(\%) = \frac{Q}{P} * 100 \,, \qquad \text{(Eq. S5)}$$

Nomenclature

Q	Heat tranfer rate, W
Cp	Specific heat, J/(Kmol.K)
T	Temperature, K
P	Power, W
I	Current, A
V	Voltage, V

EE	energy efficiency, %
Subscript	
in	Inlet
out	Outlet
ave	Average
w	water

We also investigated the stability of the Ag-coated bamboo samples for the microfluidic heater devices. We filled the bamboo-based channels with DI water and monitored the electrical resistance of the device during 9 days. The electrical measurements were done once in a day after removing from water and drying the sample. This process took less than five minutes and right after the Ag coated bamboo-based sample was immersed in water again. After 9 days, the electrical resistance increased only 16 % but even with that resistance is still below 30 ohms. It is important to mention that during the first four days the electrical resistance did not change.

H) Influence of the resin on the electrochemical experiments

As can be viewed in Figure S6, the resin layer avoids that the supporting electrolyte (blue arrows) diffuses through the bamboo structure and reaches the Ag-coated channels. In the absence of the resin, we observed peaks in the cyclic voltammogram (E ~ 0.05 V) that can be ascribed to the oxidation of the silver ink. Such peaks were not observed when the face of the bambo was coated with epoxy resin.

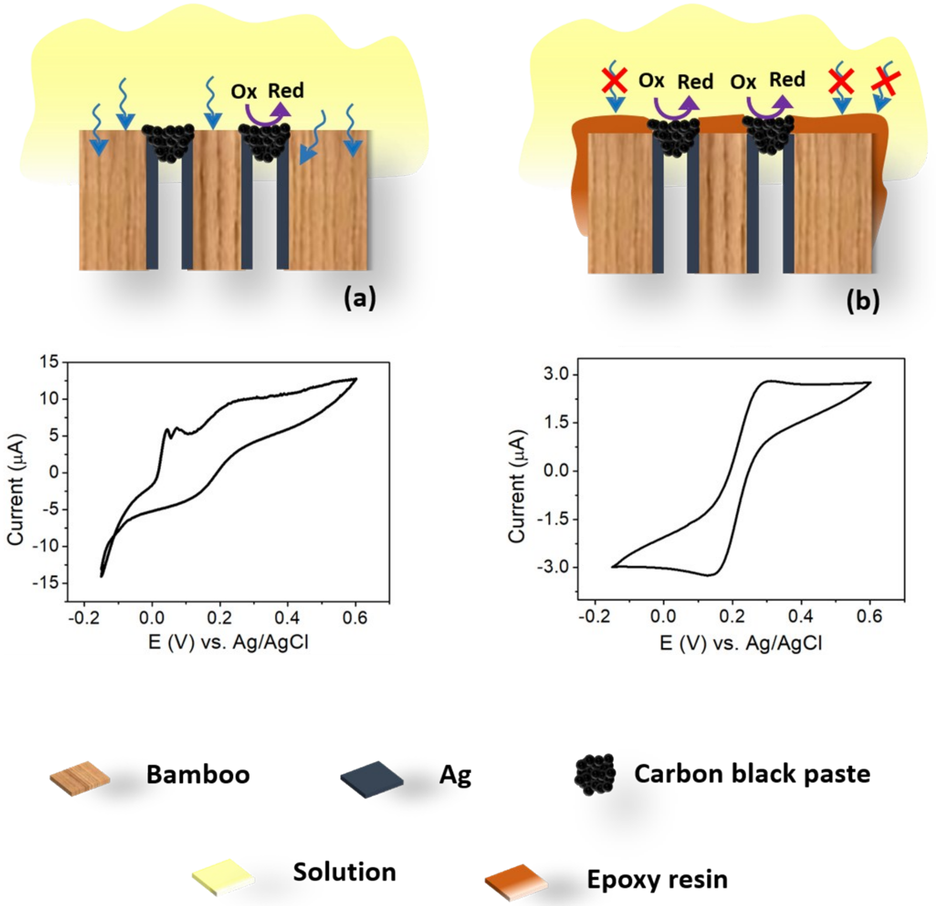

Figure S6. Schematic layout of the electrodes for (a) whithout resin and (b) with resin and their respective cyclic voltammograms obtained using 5 mM $Fe(CN)_6^{3-/4-}$ redox probe in 0.5 M KCl solution (ν = 30 mV s^{-1}).

I) Additional electrochemical experiments

Impedance experiments were obtained at the open circuit potential (0.16 V vs. Ag/AgCl for bamboo) using the $Fe(CN)_6^{3-/4-}$ redox probe, the perturbation voltage was 10 mV in frequency range from 0.1 to 10^5 Hz. Figure S7a shows the impedance spectra of the fully-integrated bamboo-based device (Bamboo-based e-cell). For comparison purposes we also added the impedance spectra of a conventional glassy carbon electrode (Conventional e-cell). As can be seen in Figure S7a, the diameter of the semi-circle using the conventional e-cell is smaller, indicating lower charge transfer resistance. However, the results obtained for the bamboo-based ecell are in the same range of other carbon-based electrodes.[13] The reason for that may arise from the composition of the carbon-paste that contains mineral oil. Mineral oil is a good binder for paste preparation, however, it has insulating properties.

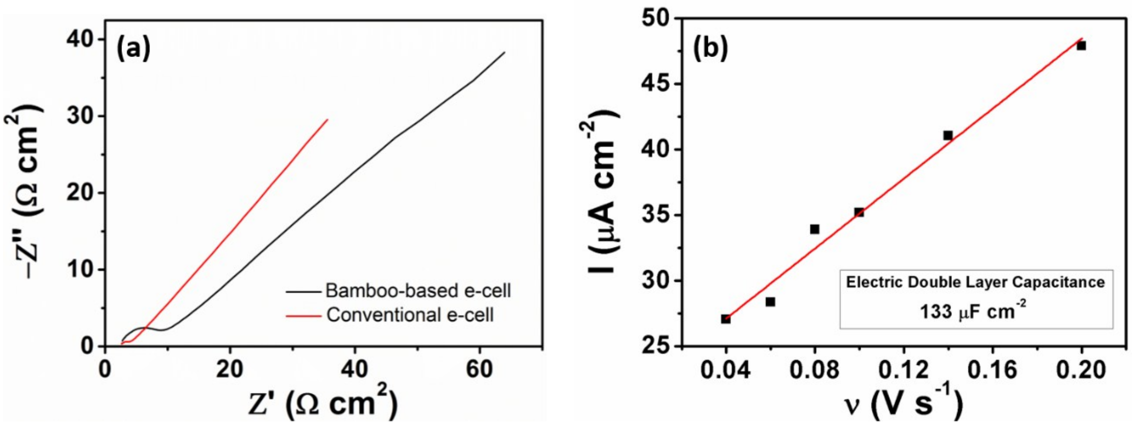

Figure S7. (a) Electrochemical impedance of the fully-integrated bamboo-based electrochemical cell and conventional electrochemical cell. The conventional e-cell was composed by polished glassy carbon electrode as working electrode, saturated calomel electrode as reference electrode and a platinum wire as counter electrode. b) Current versus scan rate curve. Conditions: KCl 0.5 M, current collected at 0.0 V vs. AgAgCl.

Cyclic voltammetry was used to obtain the capacitance of the bamboo-based e-cell. The current was collected at 0.0 V vs. Ag/AgCl at different scan rates (0.04 – 0.2 Vs^{-1}) in 0.5 M KCl solution. The width of the voltammogram ($I_{anodic} + I_{cathodic}$) was divided by the area of the electrodes and plotted versus scan rate ($V s^{-1}$), as shown in Figure S7b. The electric double layer capacitance was 133 µF cm^{-2}, which is higher when compared to conventional planar electrodes (GCE ~ 30 µF cm^{-2}, edge plane graphite ~ 60 µF cm^{-2}) but in the same range of sanded carbon electrodes containing organic binders (~150 µF cm^{-2}).[13]

References

1 M. Santhiago, C. C. Corrêa, J. S. Bernardes, M. P. Pereira, L. J. M. Oliveira, M. Strauss and C. C. B. Bufon, *ACS Appl. Mater. Interfaces*, 2017, **9**, 24365–24372.

2 M. Santhiago, P. G. da Costa, M. P. Pereira, C. C. Corrêa, V. B. de Morais and C. C. B. Bufon, *ACS Appl. Mater. Interfaces*, 2018, **10**, 35631–35638.

3 X. Li, J. Cai, Y. Shi, Y. Yue and D. Zhang, *ACS Appl. Mater. Interfaces*, 2017, **9**, 1593–1601.

4 X. Tian, M. E. Itkis, E. B. Bekyarova and R. C. Haddon, *Sci. Rep.*, 2013, **3**, 1710.

5 J. Wan, J. Song, Z. Yang, D. Kirsch, C. Jia, R. Xu, J. Dai, M. Zhu, L. Xu, C. Chen, Y. Wang, Y. Wang, E. Hitz, S. D. Lacey, Y. Li, B. Yang and L. Hu, *Adv. Mater.*, 2017, **29**, 1703331.

6 X. He, W. Gao, L. Xie, B. Li, Q. Zhang, S. Lei, J. M. Robinson, E. H. Hároz, S. K. Doorn, W. Wang, R. Vajtai, P. M. Ajayan, W. W. Adams, R. H. Hauge and J. Kono, *Nat. Nanotechnol.*, 2016, **11**, 633–638.

7 X. Li, M. Li, J. Xu, J. You, Z. Yang and C. Li, *Nat. Commun.*, 2019, **10**, 3514.

8 X. Yang, M. Sun, Y. Bian and X. He, *Adv. Funct. Mater.*, 2019, **29**, 1807615.

9 C. Teng, D. Xie, J. Wang, Z. Yang, G. Ren and Y. Zhu, *Adv. Funct. Mater.*, 2017, **27**, 1700240.

10 K. Pan, Y. Fan, T. Leng, J. Li, Z. Xin, J. Zhang, L. Hao, J. Gallop, K. S. Novoselov and Z. Hu, *Nat. Commun.*, 2018, **9**, 5197.

11 N. Behabtu, C. C. Young, D. E. Tsentalovich, O. Kleinerman, X. Wang, A. W. K. Ma, E. A. Bengio, R. F. ter Waarbeek, J. J. de Jong, R. E. Hoogerwerf, S. B. Fairchild, J. B. Ferguson, B. Maruyama, J. Kono, Y. Talmon, Y. Cohen, M. J. Otto and M. Pasquali, *Science*, 2013, **339**, 182.

12 D. W. Green and R. H. Perry, *Perry's Chemical Engineers' Handbook/edición Don W. Green y Robert H. Perry.*, .

13 K. J. Klunder, Z. Nilsson, J. B. Sambur and C. S. Henry, *J. Am. Chem. Soc.*, 2017, **139**, 12623–12631.